Confined suspension jet and long-range hydrodynamic interactions: A destabilization scenario

Alejandra Alvarez
Departamento de Física, FCFM, Universidad de Chile, Casilla 487-3, Santiago, Chile and Instituto de Innovación en Mineria y Metalurgia, IM2, avda. del Valle 738, Huechuraba, Santiago, Chile

Eric Clement
PMMH ESPCI, UMR 7636, 10 rue Vauquelin, 75231 Paris Cedex 05, France and Université Pierre et Marie Curie P6, Paris, France

Rodrigo Soto[a)]
Departamento de Física, FCFM, Universidad de Chile, Casilla 487-3, Santiago, Chile and Departamento de Física Aplicada I (Termología), Facultad de Ciencias Físicas, Universidad Complutense, 28040 Madrid, Spain

The collective dynamics of a quasi-two-dimensional suspension jet, of non-Brownian particles, confined in a thin cell and driven by gravitational force is studied both numerically and theoretically. We present a theoretical scheme aimed to describe such a system in the Stokes regime. We focus on the dynamics of the interface between the suspension and the pure fluid. Numerical simulations solving Newton's equations for all particles show that the jet free surface becomes unstable: the fastest growing modes at small sizes coarsen up to the largest structures reaching the jet lateral scale. In the bulk, structural waves develop and travel at slightly slower speed than the jet average fall. An analytical model, based on hydrodynamic-like equations for the suspension, is derived and predicts the development of the interfacial instability. It captures in essence the collective effects driving the interface destabilization, i.e., the long-range hydrodynamic interactions coupled with the abrupt interface, and no relation to surface tension is found.

I. INTRODUCTION

Understanding the dynamics of non-Brownian suspension in the low Reynolds number regime has been a long-lasting and difficult issue. Long-range hydrodynamics forces create a complex particle dynamics,[1,2] and up to now, no rigorous closed-form formulation of the problem has existed at moderate densities. For example, difficulties remain with regard to explaining particle sedimentation, dispersion, and mixing in a finite-size container (see Ref. 3 and references therein). In particular, a complete description of the collective, or macroscopic, effects that emerge from the hydrodynamics interactions is still lacking.

Recently, the miniaturization of hydrodynamics devices,[4,5] which is necessary to develop microfluidic apparatus performing at low Reynolds number, mixing, or separation, has brought to the forefront the importance of boundary confinement of suspensions. In fact, numerous devices have the form of narrow channels or Hele-Shaw cells with one direction reaching only a few particle sizes.[6,7]

Note that experimentally quasi-two-dimensional (2D) Brownian and non-Brownian suspensions have also been studied in the case in which the cell gap was almost the particle size.[8–10] These systems allow us to study simultaneously the microstructure and the individual processes as well as the collective phenomena.[11] In the case of Brownian suspensions, it has been observed that their velocity distribution is non-Gaussian[12] and they show anomalous diffusion.[10] Also, computer simulations have been used to elucidate the relation between microstructure and global flows as in sedimentation.[13] Finally, confined geometries are being used to study the collective dynamics of active suspensions.[14,15]

The flow confinement in a Hele-Shaw geometry changes the bulk hydrodynamic interaction between particles and leads to the existence of antidrag correlations due to fluid recirculation around each grain. These interactions were experimentally identified in Ref. 10 and their collective effects in the spreading of a cluster were studied in Ref. 16.

To get a better description of the mixing process that takes place in microfluidic apparatus, an important basic issue is to capture the evolution of an interface between a suspension and a particle-free fluid (the pure fluid). This problem is also related to many studies done to understand miscible interfaces dynamics, either from two different fluids[17] or a fluid in contact with a suspension falling under gravity.[18–20]

Here, we describe the evolution of the interface between a suspension and the free fluid for a jet of suspended particles in a thin cell—quasi 2D confinement—driven by gravitational forces. The suspension is non Brownian and the hydrodynamic forces between particles are obtained in the Stokes regime. Numerical simulations that solve the Newton

[a)]Electronic mail: rsoto@dfi.uchile.cl

equations for all particles follow the evolution of the jet free surfaces. We present an analytical model, based on hydrodynamic-like equations for the suspension, that is able to predict the development of the instability and its origin in the long-range forces. We present and extend a scheme that was developed recently, in the context of a 2D suspension cluster falling down[16] and also presented briefly in Ref. 21 in the context of a jet. The relative simplicity of the model, focusing on the actual effect of long-range hydrodynamic forces, allows us to discuss the dominant physical features of the interface dynamics.

II. MODEL

We consider a system of N solid particles that move through an incompressible Newtonian fluid of viscosity η. The fluid is confined between two parallel plates separated at a distance $2d$ in the z direction, being infinite in the other two directions. To simplify the computation of the hydrodynamic interaction forces, and to focus on the effect of their long-range nature, we consider cylindrical particles of height L (slightly smaller than $2d$) and diameter σ that have planar motion only. Particles are thin, i.e., $2d \ll \sigma$, and their mass is m.

The hydrodynamic forces between the cylinders in the confined geometry have been computed in Ref. 16 in the Stokes regime for a dilute suspension. First, the force over the ith particle has a drag component given by $-(m/\tau_1)\vec{u}_i$, where $\vec{u}_i$ is the in-plane velocity of particle i and $\tau_1 = md/\pi\sigma^2\eta$ is the relaxation time of a single particle. Also, the presence of the other particles induces hydrodynamic forces over each other. When particles are far apart, the force on i due to the presence of k is

$$\vec{F}_{ik}^{F} = -\frac{m}{8\tau_1}\mathbb{K}(\vec{R}_{ik})\vec{u}_k, \tag{1}$$

where $\vec{R}_{ik} = \vec{R}_i - \vec{R}_k$ is the relative distance between particles, $\vec{R}_i$ being the position of the center of mass of the ith particle and the tensor $\mathbb{K}$ is given by

$$\mathbb{K}(\vec{R}) = (\sigma/R)^2(\mathbb{I} - 2\vec{R}\vec{R}/R^2). \tag{2}$$

This force depends both on the direction of the velocity $\vec{u}_k$ and on the relative distance $\vec{R}_{ik}$. When $\vec{u}_k$ is parallel to $\vec{R}_{ik}$, the interaction force on i is parallel to $\vec{u}_k$ (drag), and if $\vec{u}_k$ is perpendicular to $\vec{R}_{ik}$, the force turns out to be in an opposite direction to $\vec{u}_k$ (antidrag).

On the other hand, when particles are close to each other, lubrication forces appear producing the net force on particle i due to the presence of k,[16]

$$\vec{F}_{ik}^{N} = 2\pi d\eta\frac{1}{\sqrt{\epsilon}}\frac{1}{R_{ik}^2}(R_{ik}^2\mathbb{I} - \vec{R}_{ik}\vec{R}_{ik})\vec{u}_{ik} + \frac{3}{2}2\pi d\eta\frac{d^2}{\sigma^2}\frac{1}{\epsilon}\frac{\vec{u}_{ik}\cdot\vec{R}_{ik}}{R_{ik}^2}\vec{R}_{ik}, \tag{3}$$

where $\epsilon = R_{ik}/\sigma - 1$ is the gap between the particles and $\vec{u}_{ik} = \vec{u}_i - \vec{u}_k$ is the relative velocity between particles. The force depends on the relative velocities between the pair and it respects the action-reaction principle. Therefore, it does not change the total momentum of the pair, but reduces the relative velocity.

The cutoff for using either expression (1) or (3) is rather arbitrary. We adopt the convention that when the pair is closer than R_{lubr}, the lubrication force (3) is used, when the distance is larger than R_{far}, the far force (1) is used, and in between a linear interpolation between the two is computed. The result is the interaction force $\vec{F}_{ik}^{I}$.

There is also an extra drag force produced by the flow between the particles and the plates.[16] This force is of the form $-\lambda\vec{u}_i$, where λ depends on the gap size and on the particular experimental setup. This term can be added to the other drag force $-m\vec{u}_i/\tau_1$, simply modifying the prefactor. In order to simplify the analysis, in what follows we will disregard the presence of this term, but in case it is relevant to some experimental configuration, it can be trivially included, modifying only quantitatively the results presented here.

In summary, the dynamical equations for the suspended particles are

$$m\frac{d\vec{u}_i}{dt} = -\frac{m}{\tau_1}\vec{u}_i + \sum_k \vec{F}_{ik}^{I} + m\vec{g}, \tag{4}$$

which constitute a complex system of equations that will be solved numerically.

Although the tensor (2) diverges at close distances, it has the remarkable property that its integral over the direction of $\vec{R}$ vanishes. This implies that if a particle is surrounded by a homogeneous distribution of suspended particles, all moving with equal velocities, the far-field contribution to the hydrodynamic force vanishes.

The long-range nature of the forces between particles makes it computationally expensive to perform direct numerical simulations where all pairs of forces are computed. However, the expressions (1) and (2) for the far-field contribution to the hydrodynamic forces suggest that a mean-field approximation can be done. In fact, if particles in a region move with similar velocities, they exert similar forces to a target particle; it is natural then to group them altogether and compute the total force made by the group on any target particle. We define the coarse-grained current $\vec{J}$ on a cell c as

$$\vec{J}_c = \frac{1}{\Delta S}\sum_{i\in c}\vec{u}_i, \tag{5}$$

where ΔS is the area of each cell.

Then, if the system is nearly homogeneous in each cell, the far-field contribution to the force (1) can be approximated by

$$\vec{F}_i = -\frac{m}{8\tau_1}\sum_c \Delta S\mathbb{K}(\vec{R}_i - \vec{R}_c)\vec{J}_c, \tag{6}$$

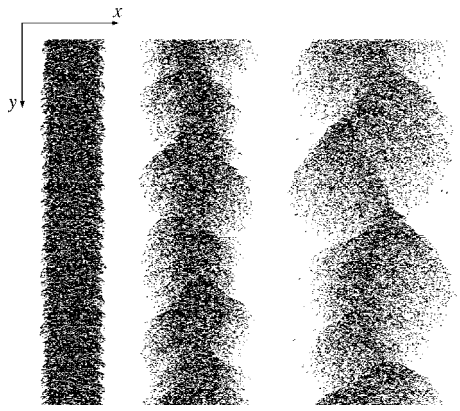

FIG. 1. Numerical simulation of a suspension jet of $N=24000$ particles falling by the action of a gravitational field. The initial size of the jet is $90\sigma\times600\sigma$. From the left to the right: $t=200$, $t=2000$, and $t=4000$. Units are described in the text.

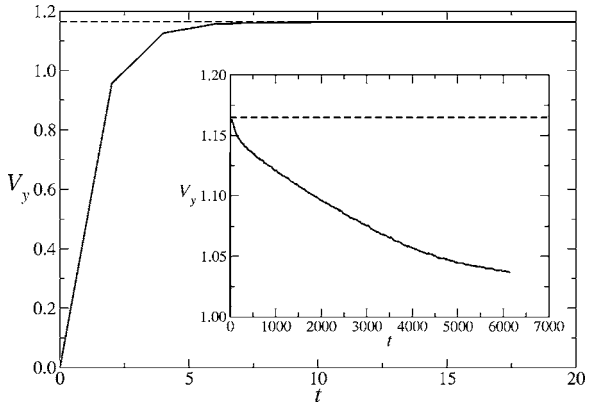

FIG. 2. Instantaneous average of the vertical velocity as a function of time (continuous line). The dashed line is the asymptotic theoretical value of the jet if it does not deform, $V_{\text{jet}}^{\infty}=1.165$. Inset: evolution for longer times.

where the sum runs on all cells and $\vec{R}_c$ is the position of the center of each cell. This expression allows us to study systems of many particles at reasonable cost. Note that the vanishing integral of $\mathbb{K}(\vec{R})$ over the angles implies that (6) can be applied down to neighboring cells without producing divergences, but the mean-field approximation can be inaccurate for near cells. Local inhomogeneities are not completely taken into account by the mean field and unrealistic vanishing forces can be obtained. To solve this problem, the mean-field approximation of the far-field force is applied only to cells that are separated by a distance larger than R_{mf}, otherwise the direct summation on the pair of particles is performed. Finally, the values chosen for performing the simulations are $R_{\text{lubr}}=1.3\sigma$, $R_{\text{far}}=2.0\sigma$, $R_{\text{mf}}=5.66\sigma$. We have tried different values for these parameters: changing R_{mf} only affects the computational speed while preserving the accuracy as shown in Ref. 16; the effect of changing R_{lubr} and R_{far} is to modify slightly the near-field dynamics, but the collective dynamics and the instability described below remain unchanged. This numerical method was shown to give accurate results in the study of the spreading of a falling cluster.[16]

III. SIMULATIONS OF A FALLING JET

The long-range forces (1) vanish when a particle is surrounded by a homogeneous medium, but in the presence of inhomogeneities the force is finite. The effect of inhomogeneities is clearly seen when there is a separation line between a region with suspended particles and a region without them; it was shown in Ref. 16 that the force is enhanced if the separation line is curved, making it possible to produce instabilities. As our description is for the dynamics of the suspended particles, and not for the surrounding fluid, it is sensible to call the separation line between a region with suspended particles and the pure fluid the *free surface*.

In order to study the effect of long range-forces on the free surfaces and, in particular, to determine if they can lead to unstable motion, we consider a falling jet of particles immersed in a fluid.

A jet of falling particles is studied numerically. Initially, a jet of $N=24000$ particles is placed randomly at rest in a rectangle of width $L_x=90\sigma$ and height $L_y=600\sigma$. They fall down due to the action of a gravitational field pointing in the positive y direction. To produce a continuous flowing jet, the vertical direction is periodic and the force computation uses the minimum image convention.[22] Alternatively, instead of the minimum image convention, a sum of all periodic images would be necessary to mimic an infinite system. Units are chosen such that the particle diameter σ, particle mass m, and the relaxation time τ_1 are set to 1. The gravitational force is $mg=1.0$ and therefore the limiting velocity for a single particle $V_1^{\infty}=g\tau_1=1.0$ [see Eq. (4)].

Figure 1 shows three successive snapshots of the jet. They show that the free surfaces become unstable, showing the appearance of waves. At the beginning the surface waves are characterized by short wavelengths, but later as the amplitude of the perturbations growth, the characteristic wavelengths grow also. A coarsening process is developed leading to larger structures. Once the size of this structure is comparable to the jet width, interactions between the two surfaces are observed and in-phase surface oscillations are obtained. Figure 1 shows also that the surface waves are also accompanied by modulations of the particle density.

Figure 2 shows the average vertical velocity of the falling jet as a function of time. It is seen that the jet rapidly gets an asymptotic velocity that is larger than the one for a single isolated particle. At much larger times, as the jet develops large structures and the particles separate, the falling velocity decreases and approaches $V_1^{\infty}=1.0$. The vertical jet velocity in the initial quasistationary state (when the jet velocity is almost constant) is homogeneous in the y direction and its dependence on x is shown in Fig. 3. It is seen that it is almost homogeneous except for small boundary effects.

To describe in more detail the coarsening process, the x-averaged density $\rho(y,t)$ and the jet width $\Delta(y,t)$ for each altitude y are studied in their time evolution. They are computed in terms of the instantaneous number particle density $n(x,y,t)$ as

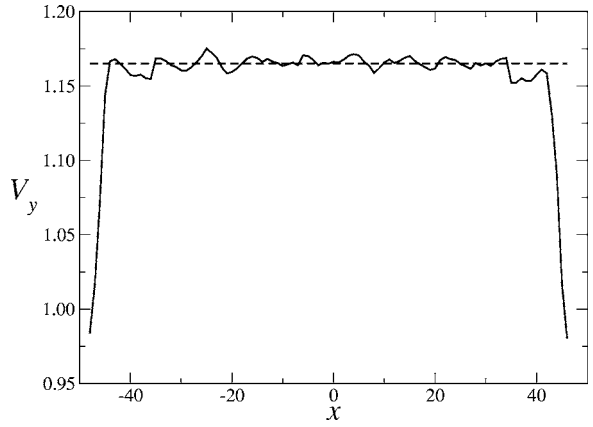

FIG. 3. Solid line: vertical velocity profile as a function of the horizontal coordinate, averaged over the vertical coordinate and in the time window $40 \leqslant t \leqslant 60$. Dashed line: average vertical velocity of the jet.

$$\rho(y,t) = \sqrt{\frac{\left[\int n(x,y,t)dx\right]^3}{12\int n(x,y,t)[x-\bar{x}(y,t)]^2 dx}}, \tag{7}$$

$$\Delta(y,t) = \sqrt{\frac{12\int n(x,y,t)[x-\bar{x}(y,t)]^2 dx}{\int n(x,y,t)dx}}, \tag{8}$$

expressions that for a rectangular density profile give precisely the average density and width, respectively. $\bar{x}(y,t)$ is the instantaneous center of mass for each altitude y. In Fig. 4, spatiotemporal plots of $\rho(y,t)$ and $\Delta(y,t)$ are presented in the reference frame falling with the same instantaneous velocity of the jet.

It is seen that besides a global jet widening and the corresponding density decrease, there are spatial modulations of the density and the width. The size of the structures associated with these modulations grows in time, showing the coarsening process. An anticorrelation between density and width is observed: the wider regions are more dilute. Also, the structures propagate in the negative y direction; as the plot is presented in the reference frame of the falling jet, it indicates that the perturbations fall at a slightly smaller velocity than the jet.

IV. GLOBAL MODEL

The behavior observed in the numerical simulations suggests an instability like that observed when two immiscible fluids in contact move with a relative velocity (Kelvin-Helmholtz instability).[23]

To describe the appearance of the surface instability, we build a global model, similar to hydrodynamic equations. We consider the particle number density $n(\vec{R})$ and the particle mean velocity $\vec{V}(\vec{R})$. The average force density over the suspension, produced by the drag force, the far force contribution (1), and the gravity acceleration is

$$\vec{F}(\vec{R}) = -\frac{1}{\tau_1}\vec{J}(\vec{R}) - \frac{1}{8\tau_1}n(\vec{R})\int d\vec{R}'\mathbb{K}(\vec{R}-\vec{R}')\vec{J}(\vec{R}') + n(\vec{R})m\vec{g}, \tag{9}$$

where $\vec{J}=mn\vec{V}$ is the mass current density.

In a Euler-like global model such as the one proposed, the lubrication force contribution can be neglected because its effect is to reduce velocity fluctuations, but it does not modify the mean velocity as it only affects the relative velocity. Eventually, its effect would be to produce an additional effective viscosity as obtained in kinetic theory.[24]

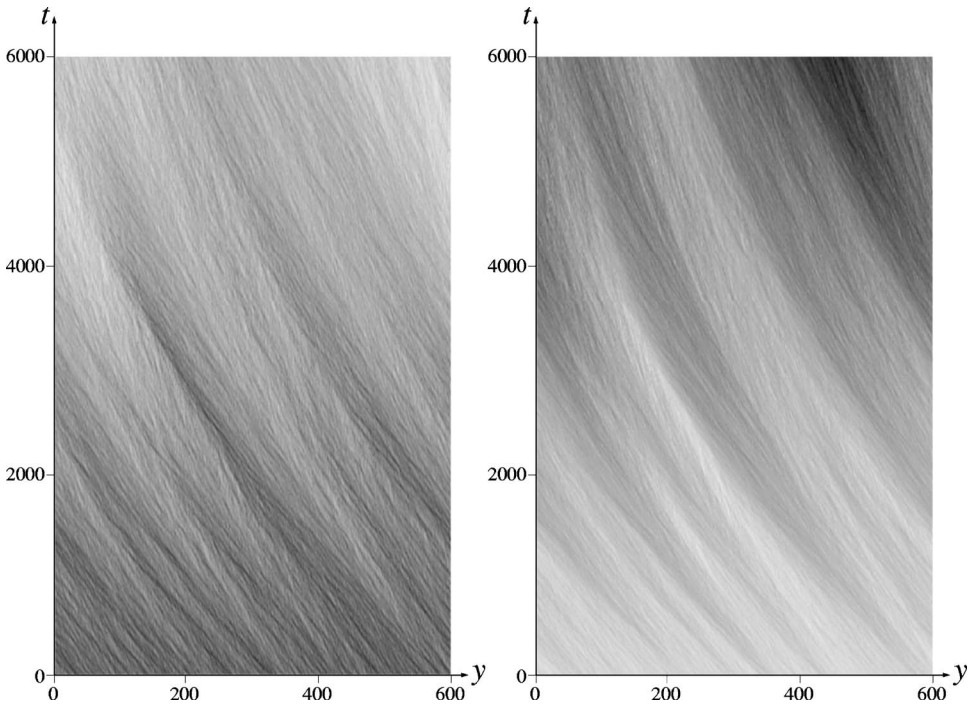

FIG. 4. Spatiotemporal diagrams of the average density $\rho(y,t)$ (left) and the jet width $\Delta(y,t)$ (right) in the reference frame of the falling jet. Time is on the vertical axis and increasing upward. The horizontal axis is the y coordinate, with periodic boundary conditions, and the gravitational acceleration points to the right. The gray scale is proportional to the value, with lighter regions representing smaller values. The minimum and maximum represented densities are $\rho^{\min}=0.041$ and $\rho^{\max}=0.707$, respectively, and the minimum and maximum represented widths are $\Delta^{\min}=50$ and $\Delta^{\max}=346$, respectively. The simulation parameters are the same as in Fig. 1 and the total simulation time is $t=6152$.

Therefore, the global equations of motion for the suspension can be written as

$$\frac{\partial n}{\partial t} + \nabla \cdot (n\vec{V}) = 0, \tag{10}$$

$$nm\left(\frac{\partial \vec{V}}{\partial t} + \vec{V} \cdot \nabla \vec{V} \right) = \vec{F}. \tag{11}$$

Before analyzing the development of the instabilities, let us consider the evolution of an unperturbed homogeneous jet. For a thin jet of width L_x and height L_y, with periodic boundary conditions in y, if the particle current is assumed to be homogeneous $\vec{J}(\vec{R},t)=J_{\text{jet}}(t)\hat{y}$, the integral term in (9) is almost independent of x and can be well approximated by [see Eq. (A2)]

$$\int d\vec{R}'\,\mathbb{K}(\vec{R}-\vec{R}')\vec{J}_{\text{jet}} = 2\sigma^2[\arctan(L_y/L_x) - \arctan(L_x/L_y)]J_{\text{jet}}\hat{y}, \tag{12}$$

independent of $\vec{R}$. Therefore, Eqs. (10) and (11) admit a solution of an approximately homogeneous falling jet, with velocity

$$V_{\text{jet}}(t) = g\tau_{\text{jet}}(1 - e^{-t/\tau_{\text{jet}}}), \tag{13}$$

where the jet relaxation time is

$$\tau_{\text{jet}} = \frac{\tau_1}{1 - n_0\sigma^2[\arctan(L_y/L_x) - \arctan(L_x/L_y)]/4} \tag{14}$$

and n_0 is the jet number density. The homogeneity of the jet velocity is verified in the simulation as shown in Fig. 3.

Note that the asymptotic velocity and the relaxation time are different from the ones of a single falling particle, τ_1 and $V_1^\infty = g\tau_1$, respectively. A peculiar feature is that the modification of the falling velocity depends only on the system shape, but not on its size. A similar phenomenon was observed in the case of a falling circular cluster.[16] In fact, this effect is due to the tensorial behavior shown by the hydrodynamic interactions [Eqs. (1) and (2)]. For a thin jet ($L_x < L_y$), the particles are located such that most of their relative distances are parallel to the falling velocity. Equation (1) indicates that particles exert a positive drag, in the direction of the motion, increasing the falling velocity. On the other hand, if the jet were wide ($L_x > L_y$), most of the relative distances between particles would be perpendicular to the falling velocity, and the dominant contribution of the hydrodynamic forces would be the antidrag, reducing the jet falling velocity. In the case of the jet we are considering, the theoretical values for the falling jet velocity and relaxation time are $V_{\text{jet}}^\infty = 1.165$ and $\tau_{\text{jet}} = 1.165$, which are larger than the values for a single particle. In Fig. 2 it is seen that the jet rapidly gets this velocity, and afterward, when it starts deforming, the velocity slowly decreases approaching $V_1^\infty = 1.0$. This long-time value is consistent with Eqs. (13) and (14) when the jet density decreases. An exponential fit to the early-time evolution of the velocity of the jet gives the same relaxation time as predicted.

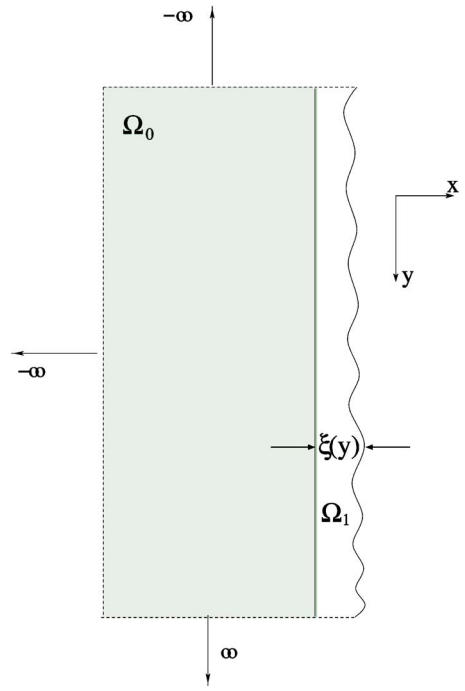

FIG. 5. Sketch of the semi-infinity suspension. Ω_o is the unperturbed domain, Ω_1 is the perturbation domain, and ξ is the perturbation in the x direction.

In the presence of a free surface, an additional equation must be added to describe the evolution of the free surface position $\xi(y,t)$ (see Fig. 5). The mean suspension velocity at the surface must be equal to the surface velocity[23]

$$\frac{\partial \xi}{\partial t} + V_y\Big|_{x=\xi} \frac{\partial \xi}{\partial y} = V_x\Big|_{x=\xi}. \tag{15}$$

V. LINEAR STABILITY ANALYSIS

The stability of the free surface of the jet is analyzed using the global equations (10), (11), and (15). To simplify the problem and assuming that at the beginning the two free surfaces do not interact strongly, we will consider the simpler case of a single free surface, limiting a semi-infinite homogeneous suspension in the $x<0$ region, of density n_0. In this geometry, the velocity of the unperturbed jet is exactly independent of x, taking the value $\vec{V}_0 = g\tau_1\hat{y}/(1+\beta_0/4)$, where $\beta_0 = \pi\sigma^2 n_0/4$ is the area fraction of the suspension [see Eq. (A3)]. Note that in this geometry $V_0 < V_1^\infty$.

We consider small perturbations of the free surface. Introducing a formal parameter $\epsilon \ll 1$, the fields are written as $\vec{V}(\vec{R}) = \vec{V}_0 + \epsilon\vec{V}_1(\vec{R})$, $n = n_0 + \epsilon n_1(\vec{R})$, and $\xi = \epsilon\xi_1(y)$. The domain Ω over which the integration in (9) must be done is split into the initial domain $\Omega_0: x \leqslant 0$, plus a perturbation domain $\Omega_1: 0 < x \leqslant \xi(y,t)$ (see Fig. 5). Keeping terms up to linear order in ϵ, the equations read

$$\frac{\partial n_1}{\partial t} + \nabla \cdot (n_0\vec{V}_1 + n_1\vec{V}_0) = 0, \tag{16}$$

$$\frac{\partial \vec{V}_1}{\partial t} + \vec{V}_0 \cdot \nabla \vec{V}_1 = -\frac{1}{\tau_1}\vec{V}_1(\vec{R}) - \frac{1}{8\tau_1}\int_{\Omega_0} d\vec{R}'\,\mathbb{K}(\vec{R}-\vec{R}') \times [n_0 \vec{V}_1(\vec{R}') + n_1(\vec{R}')\vec{V}_0] - \frac{1}{8\tau_1}\int_{-\infty}^{\infty} dy'\,\mathbb{K}(\vec{R}-y'\hat{y})n_0\vec{V}_0\xi(y'), \tag{17}$$

$$\frac{\partial \xi}{\partial t} + V_{0y}\bigg|_{x=0}\ \frac{\partial \xi}{\partial y} = V_{1x}\bigg|_{x=0}. \tag{18}$$

The deformed surface has a long-range effect of the fluid motion, as reflected by the last term in Eq. (17).

This integro-differential system of equations does not have an evident analytic solution. However, an estimation of the instability modes can be obtained as follows. A Fourier expansion of the fields $A_1(\vec{R},t)=\hat{A}_1(\vec{k},t)e^{i\vec{k}\cdot\vec{R}}$ is performed. As the Fourier basis is not a solution of the system [particularly because of the integral terms in (17)], we obtain an estimation by evaluating the equations at $x=0$. Defining dimensionless variables $\rho=n_1/n_0$, $\vec{U}=\vec{V}_1/(g\tau_1)$, $\varphi=\xi/(g\tau_1^2)$, $\vec{q}=(g\tau_1^2)\vec{k}$, and $s=t/\tau_1$, the equations read

$$\frac{\partial \rho}{\partial s} = -i\vec{q}\cdot\vec{U} - i\vec{q}\cdot\vec{U}_0\rho, \tag{19}$$

$$\frac{\partial \vec{U}}{\partial s} = -\vec{U} - i(\vec{q}\cdot\vec{U}_0)\vec{U} - \mathbb{Q}_1(\vec{U}+\rho\vec{U}_0) - \mathbb{Q}_2\vec{U}_0\varphi, \tag{20}$$

$$\frac{\partial \varphi}{\partial s} = U_x - i(\vec{q}\cdot\vec{U}_0)\varphi, \tag{21}$$

with the following defined tensors [see Eq. (A5)]:

$$\mathbb{Q}_1 = \frac{\beta_0}{2}\left\{\begin{pmatrix}1 & 0\\ 0 & -1\end{pmatrix} + \frac{|q_y|}{iq_x+|q_y|}\begin{pmatrix}-1 & i\\ i & 1\end{pmatrix}\right\}, \tag{22}$$

$$\mathbb{Q}_2 = \frac{\beta_0}{2}|q_y|\begin{pmatrix}-1 & i\\ i & 1\end{pmatrix}. \tag{23}$$

We recall that the dimensionless jet falling velocity is $\vec{U}_0 = \hat{y}/(1+\beta_0/4)$.

The tensors $\mathbb{Q}_1$ and $\mathbb{Q}_2$ capture the effect of the long-range forces produced by the perturbations, when they are integrated in the semi-infinite volume. $\mathbb{Q}_1$ describes the interaction of the perturbations with the bulk and $\mathbb{Q}_2$ the interaction with the free surface. Remarkably, $\mathbb{Q}_2$ is proportional to q and not to q^2, therefore the effect of a curved surface cannot be described in terms of an effective surface tension. Note also that $\mathbb{Q}_1$ is independent of the magnitude of $\vec{q}$ and depends only on its direction. This fact has an important consequence because in the limit of perturbations of small wave vectors the effect of the hydrodynamic interactions does not vanish. In fact, in the limit $q\to 0$ the linear system of equations (21) has a Jordan-block structure and admits a solution of the form (at first order in β_0)

$$\rho = 2AU_0^{-1}(-\cos\phi + i|\sin\phi|), \tag{24}$$

$$U_x = A\beta_0|\sin\phi|, \tag{25}$$

$$U_y = -A\beta_0\cos\phi, \tag{26}$$

$$\varphi = A\beta_0|\sin\phi|t, \tag{27}$$

where A is an arbitrary coefficient given by the initial condition and ϕ is the angle between the wave vector $\vec{q}$ and the $\hat{x}$ direction. The solution shows a linear, instead of exponential, increase in time of the surface oscillations.

For larger values of q, the system of equations loses its Jordan-block structure and solutions in the form $\exp(\lambda s)$ are looked for. The eigenvalues λ for $q\ll 1$, $\beta_0\ll 1$, and $0<\phi<\pi$ ($\sin\phi>0$) are

$$\lambda_1 = -iU_0q(1+\beta_0/4)\sin\phi + \frac{\sqrt{3}}{4}\beta_0U_0q\sin\phi + O(q^2), \tag{28}$$

$$\lambda_2 = -iU_0q(1+\beta_0/4)\sin\phi - \frac{\sqrt{3}}{4}\beta_0U_0q\sin\phi + O(q^2), \tag{29}$$

$$\lambda_3 = -1 - \frac{\beta_0}{2}(\cos\phi + i\sin\phi) + O(q), \tag{30}$$

$$\lambda_4 = -1 + \frac{\beta_0}{2}(\cos\phi + i\sin\phi) + O(q), \tag{31}$$

and similar results for $\pi<\phi<2\pi$ ($\sin\phi<0$).

Two of the eigenvalues, λ_3 and λ_4, have negative real parts for small q and therefore correspond to damped motion. However, the real part of λ_1 (λ_2 for $\pi<\phi<2\pi$) is positive. Therefore, an instability is predicted. The analysis shows that the system becomes unstable for any strength of the gravitational force and, coming back to the original units, the instability rate is directly proportional to V_0k. In the limit $k\ll 1$, the real parts of λ_1 and λ_2 are proportional to the wave vector. It is reasonable to expect that a more detailed model, including terms proportional to gradients of $\vec{V}$ or the viscous effect due to the lubrication forces, will mean that for high enough wave vectors, the real part of the eigenvalues becomes negative again. Hence, it is expected that the system is unstable for a range of wave vectors going from zero to a finite value, showing the coarsening process observed in the simulation.[25]

The eigenvalues λ_1 and λ_2 also have an imaginary part. The dominant one with respect to q and β_0 is $\lambda_{1I}=-iqU_0(1+\beta_0/4)\sin\phi$. It corresponds to a wave in the form $\exp\{iq\sin\phi[y-U_0(1+\beta_0/4)t]+iq\cos\phi x\}$, which propagates in the $+y$ direction, with phase velocity $U_0(1+\beta_0/4)=1$. That is, the structures propagate at the same velocity as a single falling particle. This phase velocity is larger than the jet falling velocity by a factor $O(\beta_0)$. As a consequence, the unstable structures should move faster than the jet. In the simulations, we actually find the opposite: the structures move slower than the jet. This change of character can be due to the different geometries that are considered, as it also

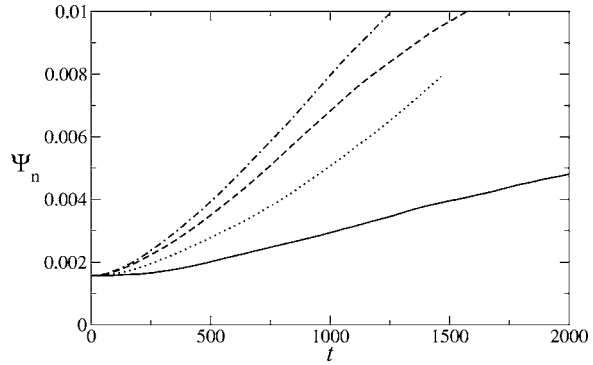

FIG. 6. Evolution of the Fourier amplitudes Ψ_n computed with the same wave number n as the perturbation made on the surface. $n=1$, continuous line; $n=2$, dotted line; $n=3$, dashed line; and $n=4$, dash-dotted line.

happens to the jet falling velocity that in one case is faster than V_1^∞, while in the other case was found slower.

The linear stability analysis for a jet with two free surfaces as in the simulations is much more involved. One extra equation must be added and the long-range interactions in this geometry give more complex expressions, as can be seen in the case of the falling velocity. Nevertheless, we expect that the analysis presented here, showing that the surface is unconditionally unstable and the growth rates are proportional to the wave vectors, is preserved.

We have studied numerically the growth rate for different wave vectors in the jet. For each wave vector we have performed new simulations, with an initial condition similar to the one described previously for the jet except that the x coordinates are modulated in such a way as to create two waves of vectors $k_y=2\pi n_y/L_y$ in the surface positions. In practice, we map the initial x coordinates of the original rectangular jet as $[0,L_x]\rightarrow[-A\cos(k_y y),L_x+A\cos(k_y y)]$. In each simulation, we compute the evolution of the Fourier amplitudes $\Psi_n=N^{-1}|\Sigma_i(x_i-L_x/2)^2 e^{2\pi i n y_i/L_y}|=N^{-1}|\int\rho(x,y)(x-L_x/2)^2 e^{2\pi i n y/L_y}|$ with the same wave number as the initial perturbation. These Fourier amplitudes measure, at linear order, the amplitude of $\xi(k_y)$. Figure 6 shows the results of the Fourier amplitudes for the simulations done with $n_y=1,2,3,4$. For $n_y=1$, a linear increase of Ψ is observed while for $n_y\geqslant 2$, an exponential increase of the Ψ's are obtained, until nonlinear interaction between modes appears. The growth rates are $\lambda(n_y=2)=1.21\times10^{-3}$, $\lambda(n_y=3)=1.82\times10^{-3}$, and $\lambda(n_y=4)=2.19\times10^{-3}$, which are roughly in the ratio 2:3:4, confirming the linear proportionality with k. However, no direct comparison with the prediction can be made because only k_y was fixed but not k_x, therefore the angle ϕ takes all possible values. Larger values of n_y give very noisy results.

VI. CONCLUSIONS

In conclusion, we investigated the dynamical evolution, in the Stokes regime, of a jet of falling particles confined in a Hele-Shaw cell. The free surfaces of the jet are shown to become unstable and a coarsening process takes place from the smallest sizes up to the largest structures.

A continuous Euler-like hydrodynamic model for the suspension is presented that describes the main features of the jet flow. In particular, the model predicts a geometry-dependent falling velocity for the jet (thin jets fall faster than thick jets).

The theoretical analysis shows that the free surface is unstable to any gravitational force and any wave vector. The growth rates are proportional to the wave vectors, a result that is consistent with the coarsening process observed in the simulations. Finally, the model predicts that the structures move with a velocity slightly different from the jet's velocity, as observed in the simulations but with a different sign prediction. In this problem, we find that the interface dynamics is quite different from the usual immiscible fluid case in which the surface tension plays a leading role such as to select and stabilize structures. For the present jet, the particle hydrodynamic interactions create a surface instability essentially due to long-range effects caused by flow recirculation around a particle. A crucial point is that this effect is scale-free. We observe at the end of the simulations a partial mixing due to flow structuration as well as hydrodynamic dispersion causing a diffuse interface.

Finally, we pose a question on the relation between this model and the dynamics of actual non-Brownian suspensions in a confined cell. Although we have here a situation that is a bit artificial as the problem is solved in the case of particle sizes (diameter) larger than the cell gap, we believe that all the features dealing with scales larger than the gap (essentially the long-range interactions) will survive at the qualitative level.

ACKNOWLEDGMENTS

The authors thank P. Cordero and M. Malek Mansour for their comments. A.A. and R.S. are grateful for the hospitality of CECAM, ENS-Lyon where part of this work was done. The simulations were done in the CIMAT's parallel cluster. This work has been partly financed by the *Fondecyt* Research Grant No. 1030993, the ECOS-Conicyt Research Grant No. C03E05, and the *Fondap* Grant No. 11980002. A.A. acknowledges the financial support of a *Mecesup* grant.

APPENDIX: KERNEL INTEGRALS

Some integrals of the kernel $\mathbb{K}(\vec{R})$ (2) used in the manuscript are as follows:

(a) Homogeneous integral for the jet,

$$I_1=\int_{-L_x}^{L_x}dx'\int_{-L_y}^{L_y}dy'\,\mathbb{K}(\vec{R}-\vec{R}')$$
$$=2\sigma^2\left[\arctan\left(\frac{L_y}{L_x-x}\right)-\arctan\left(\frac{L_x+x}{L_y}\right)\right]\begin{pmatrix}1&0\\0&-1\end{pmatrix}, \quad \text{(A1)}$$

where $\vec{R}=x\hat{x}+y\hat{y}$ is any vector in the interior of the integration domain and we have used periodic boundary conditions in y, with the minimum image convention, consistently with the simulations. When $L_y\gg L_x$, the integral depends slightly on x and its horizontal average is in that limit

$$I_1 \approx 2\sigma^2[\arctan(L_y/L_x) - \arctan(L_x/L_y)]\begin{pmatrix}1 & 0\\ 0 & -1\end{pmatrix} + \mathcal{O}[(L_x/L_y)^3]. \quad \text{(A2)}$$

(b) Homogeneous integral for the semi-infinite system,

$$I_2 = \int_{-\infty}^{0} dx' \int_{-\infty}^{\infty} dy' \mathbb{K}(\vec{R} - \vec{R}') = -\frac{\pi\sigma^2}{2}\begin{pmatrix}1 & 0\\ 0 & -1\end{pmatrix}, \quad \text{(A3)}$$

with $\vec{R}=x\hat{x}+y\hat{y}$ any vector with $x<0$ and we have used periodic boundary conditions in y.

(c) Fourier transform for the semi-infinite system,

$$I_3 = \int_{-\infty}^{0} dx' \int_{-\infty}^{\infty} dy' \mathbb{K}(\vec{R} - \vec{R}') e^{i\vec{k}\cdot\vec{R}'} = \pi\sigma^2\left[\begin{pmatrix}1 & 0\\ 0 & -1\end{pmatrix} + \frac{|k_y|}{ik_x + |k_y|}\begin{pmatrix}-1 & i\\ i & 1\end{pmatrix}\right], \quad \text{(A4)}$$

with $\vec{R}=x\hat{x}+y\hat{y}$ any vector with $x<0$ and we have used periodic boundary conditions in y.

(d) Fourier transform for the interface line,

$$I_4 = \int_{-\infty}^{\infty} dy \mathbb{K}(x\hat{x} + y\hat{y}) e^{iky} = \pi\sigma^2\left\{\delta(x)\begin{pmatrix}1 & 0\\ 0 & -1\end{pmatrix} + |k|e^{-|kx|}\begin{pmatrix}-1 & i\\ i & 1\end{pmatrix}\right\}. \quad \text{(A5)}$$

The Dirac delta appears when $\mathbb{K}$ is evaluated up to the origin, which physically cannot happen because the interaction is replaced by the lubrications forces. Therefore, this term will be eliminated in the evaluation of the kernel integrals.

[1] J. Happel and H. Brenner, *Low Reynolds Number Hydrodynamics, with Special Applications to Particulate Media* (Prentice-Hall, London, 1965).

[2] J. F. Brady and G. Bossis, "Stokesian dynamics," Annu. Rev. Fluid Mech. **20**, 111 (1988).

[3] A. J. C. Ladd, "Effect of container walls on the velocity fluctuations of sedimenting spheres," Phys. Rev. Lett. **88**, 048301 (2002).

[4] S. Kim and S. J. Karrila, *Microhydrodynamics: Principles and Selected Applications*, Series in Chemical Engineering (Butterworth-Heinemann, Stoneham, 1991).

[5] H. A. Stone, A. D. Stroock, and A. Ajdari, "Engineering flows in small devices: Microfluidics towards a lab-on-chip," Annu. Rev. Fluid Mech. **20**, 111 (2004).

[6] B. H. Weigl and P. Yager, "Microfluidic diffusion-based separation and detection," Science **283**, 346 (1999).

[7] G. M. Whitesides and A. D. Stroock, "Flexible methods for microfluidics," Phys. Today **54**(6), 42 (2001).

[8] F. Rouyer, J. Martin, and D. Salin, "Structure, density, and velocity fluctuations in quasi-two-dimensional non-Brownian suspensions of spheres," Phys. Rev. Lett. **83**, 1058 (1999).

[9] J. Santana-Solano and J. Arauz-Lara, "Hydrodynamic interactions in quasi-two-dimensional colloidal suspensions," Phys. Rev. Lett. **87**, 038302 (2001).

[10] B. Cui, "Anomalous hydrodynamic interaction in a quasi-two-dimensional suspension," Phys. Rev. Lett. **92**, 258301 (2004).

[11] A. H. Marcus, J. Schofield, and S. A. Rice, "Experimental observations of non-Gaussian behavior and stringlike cooperative dynamics in concentrated quasi-two-dimensional colloidal liquids," Phys. Rev. E **60**, 5725 (1999).

[12] F. Rouyer, J. Martin, and D. Salin, "Non-Gaussian dynamics in quasi-two-dimensional noncolloidal suspensions," Phys. Rev. Lett. **83**, 1058 (1999).

[13] E. Kuusela, J. M. Lahtinen, and T. Ala-Nissila, "Sedimentation dynamics of spherical particles in confined geometries," Phys. Rev. E **69**, 066310 (2004).

[14] X.-L. Wu and A. Libchaber, "Particle diffusion in a quasi-two-dimensional bacterial bath," Phys. Rev. Lett. **84**, 3017 (2000).

[15] J. P. Hernandez-Ortiz, C. G. Stoltz, and M. D. Graham, "Transport and collective dynamics in suspensions of confined swimming particles," Phys. Rev. Lett. **95**, 204501 (2005).

[16] A. Alvarez and R. Soto, "Dynamics of a suspension confined in a thin cell," Phys. Fluids **17**, 093103 (2005).

[17] P. Petitjeans, C. Y. Chen, E. Meiburg, and T. Maxworthy, "Miscible quarter five-spot displacements in a Hele-Shaw cell and the role of flow-induced dispersion," Phys. Fluids **11**, 1705 (1999).

[18] J. M. Nitsche and G. K. Batchelor, "Break-up of a falling drop containing dispersed particles," J. Fluid Mech. **340**, 161 (1997).

[19] G. Machu, W. Meile, L. C. Nitsche, and U. Schaflinger, "Coalescence, torus formation and breakup of sedimenting drops: Experiments and computer simulations," J. Fluid Mech. **447**, 299 (2001).

[20] M. Nicolas, "Experimental study of gravity-driven dense suspension jets," Phys. Fluids **14**, 3570 (2002).

[21] A. Alvarez, R. Soto, and E. Clement, "Free surface instability in a confined suspension jet," Physica A **356**, 196 (2005).

[22] M. P. Allen and D. J. Tildesley, *Computer Simulation of Liquids* (Oxford Science, New York, 1990).

[23] S. Chandrasekhar, *Hydrodynamic and Hydromagnetic Stability*, International Series of Monographs on Physics (Dover, Oxford, 1981).

[24] S. Chapman and T. G. Cowling, *The Mathematical Theory of Non-Uniform Gases*, 3rd ed. (Cambridge University Press, New York, 1970).

[25] P. Politi and C. Misbah, "When does coarsening occur in the dynamics of one-dimensional fronts?" Phys. Rev. Lett. **92**, 090601 (2004).